Higher order decouplings of the dilated electron propagator with applications to 2 P Be − , 2 P Mg − shape and 2 S Be + (1s −1) Auger resonances

Arun Venkatnathan, S. Mahalakshmi, and Manoj K. Mishra

Citation: The Journal of Chemical Physics **114**, 35 (2001); doi: 10.1063/1.1328395
View online: http://dx.doi.org/10.1063/1.1328395
View Table of Contents: http://scitation.aip.org/content/aip/journal/jcp/114/1?ver=pdfcov
Published by the AIP Publishing

Higher order decouplings of the dilated electron propagator with applications to $^2P\,Be^-$, $^2P\,Mg^-$ shape and $^2S\,Be^+$ $(1s^{-1})$ Auger resonances

Arun Venkatnathan, S. Mahalakshmi, and Manoj K. Mishra
Department of Chemistry, Indian Institute of Technology, Bombay Powai, Mumbai 400 076, India

(Received 1 August 2000; accepted 3 October 2000)

The full third order (Σ^3), quasi-particle third order (Σ_q^3) and Outer Valence Green's Function decouplings of the bi-orthogonal dilated electron propagator have been implemented for the first time and results from their application to $^2P\,Be^-$, $^2P\,Mg^-$ shape and $^2S\,Be^+$ $(1s^{-1})$ Auger resonances are presented and compared with energies and widths obtained using the zeroth order (Σ^0), quasi-particle second order (Σ_q^2) and second order (Σ^2) decouplings. The energies and widths from third order decoupling for shape resonances are close to those obtained using second order self-energy approximants. The energy and width calculated using the third order decoupling for Auger resonances provide better agreement with experimental results, with the much more economic quasi-particle third order decoupling being just as effective. The differences between FDAs from different decouplings are analyzed to elicit the role of correlation and relaxation in the formation and decay of shape and Auger resonances. © *2001 American Institute of Physics.*
[DOI: 10.1063/1.1328395]

I. INTRODUCTION

Electron propagator theory[1–6] has emerged as an effective tool for accurate calculation of ionization potentials and electron affinities. The dilated[7,8] electron propagator[9–11] where all electronic coordinates in the Hamiltonian have been scaled by a complex factor $\eta=\alpha e^{i\theta}$ has been successfully employed to elicit the energy and width of electron scattering shape and Auger resonances.[12] The calculation of resonance energy and width from the resonant poles of the dilated electron propagator is demanding since these are identified by constructing the dilated electron propagator for a large number of η values ($\sim$5–10 α and $\sim$30 θ values per α being typically representative) and associating the poles invariant to changes in η with resonances.[7–11] The treatment of resonances using the dilated electron propagator is therefore $\sim$150 times more arduous compared to an equivalent real electron propagator calculation of ionization potential and electron affinity. For this reason, although the use of the third order decoupling has become routine in calculation of ionization potentials/electron affinities, the treatment of resonances using the dilated electron propagator method has been limited to the use of second or pseudo-second order (diagonal $2ph$-TDA) decouplings and their quasi-particle variants.[12–14]

The second order dilated electron propagator provides resonance energies which are in fairly good agreement with those from experiment and other theoretical methods but for many systems, the widths of the shape resonances are much narrower than those observed experimentally.[12] The diagonal $2ph$-TDA decoupling[15–17] includes diagonal ring and ladder diagrams to all orders but does not seem to provide much improvement.[18] Further accuracy in the treatment of resonances therefore requires an exploration of improvements available from third and other higher order decouplings; More so, since the use of third order decoupling has offered considerable improvement in the accuracy of calculated ionization energies.[19] Also, with the advent of faster computers with larger memory and storage space, it has become possible to perform third order calculations for the dilated electron propagator as well and an examination of the effect of higher order decouplings like the third order (Σ^3), Outer Valence Green's Function (OVGF), quasi-particle third order (Σ_q^2) on the resonance attributes of the prototypical $^2P\,Be^-$, $^2P\,Mg^-$ shape resonances and the $^2S\,Be^+$ $(1s^{-1})$ Auger resonance is the principal focus of this paper. The Feynman–Dyson Amplitudes (FDAs) of the electron propagator serve as correlated orbitals[20] and the radial probability density profiles of the resonant FDAs from different decouplings are analyzed to understand the role of relaxation and correlation in formation and decay of shape and Auger resonances.

The formal developments of the bi-orthogonal dilated electron propagator based on bi-variational SCF[21] closely follow the derivation of different decouplings for the real electron propagator[1,3,6,22] and only a skeletal outline is offered in Sec. II for completeness. The effect of correlation and relaxation using the third order, quasi-particle third order and OVGF decouplings of the dilated electron propagator on resonance at tributes are presented in Sec. III. A summary of main results in Sec. IV concludes this paper.

II. METHOD

The dilatation of all the electronic coordinates ($\mathbf{r}\rightarrow\eta\mathbf{r};\eta=\alpha e^{i\theta}$) in the system Hamiltonian leads to $H^{\dagger}(\eta)=H(\eta^*)=H(\eta^*)\neq H(\eta)$, i.e., $H(\eta)$ is non-Hermitian and the variational theorem does not apply. However, there exists a bi-variational theorem[23,24] for non-Hermitian operators. The bi-variational SCF equations for the dilated Hamiltonian are derived by extremizing the generalized functional

$$\mathcal{E}(\Phi_0,\Psi_0)=\frac{\langle\Phi_0|H(\eta)|\Psi_0\rangle}{\langle\Phi_0|\Psi_0\rangle} \tag{1}$$

under the constraint that solutions Φ_0 and Ψ_0 be the single determinantal approximation to the exact N electron eigenfunctions $|\tilde{N}\rangle$ and $|N\rangle$ of the $H^\dagger(\eta)$ and $H(\eta)$, respectively, and the constituent one-electron orbitals $\{\phi\}$ and $\{\psi\}$ be bi-orthogonal, i.e., $\langle\phi_i|\psi_j\rangle=\delta_{ij}$. The Grassmann Algebra G associated with field operators defined on $\{\phi\}$ has an adjoint algebra G^* associated with $\{\phi\}$, and in terms of the duality between G and G^*, the interior multiplication of the left $\rfloor$, and of the right $\lfloor$, are defined as follows:

$$(\chi,a_i\wedge\xi)=\langle\chi(a_i\wedge)^\dagger,\xi\rangle=\langle\chi\rfloor a_i,\xi\rangle, \tag{2}$$

with χ, $\chi\rfloor a_i\in G^*$ and ξ, $a_i\wedge\xi\in G$. Similarly, we have

$$\langle\chi\wedge a^i,\xi\rangle=\langle\chi,(\wedge a^i)^\dagger\xi\rangle=\langle\chi,a^i\lfloor\xi\rangle \tag{3}$$

with χ, $\chi\wedge a^i\in G^*$ and ξ, $a^i\lfloor\xi\in G$.

The interior multiplications $a^i\lfloor$ and $\rfloor a_i$ decrease the rank of tensors in G and G^*, respectively. It is obvious that the exterior multiplications $a_i\wedge$ and $\wedge a^i$ and the interior multiplications $a^i\lfloor$ and $\rfloor a_i$ may be formalized as the familiar creation and annihilation operators on the direct $\{\psi_i\}$ and adjoint $\{\phi_i\}$ spaces, respectively, except that now the operators and their adjoints do not have the same domain. Specifically $(a_i\wedge)^\dagger=\rfloor a_i$. These concepts are part of the general theory of Dual Grassmann Algebra.[25] Some other relevant results are:

$$(a_i\wedge)^\dagger=\rfloor a_i\quad (a^i\lfloor)^\dagger=\wedge a^i, \tag{4}$$

$$[a^i\lfloor,a^j\lfloor]_+=0=[a_i\wedge,a_j\wedge]_+;\quad [a_i\wedge,a^j\lfloor]_+=\delta_{ij}. \tag{5}$$

The electron field operator $\hat{\psi}(x)$ for the direct space is given by

$$\hat{\psi}(x)=\sum_i\ \psi_i(x)a^i\lfloor=\sum_i\ \psi_i(x)(\wedge a^i)^\dagger,$$

and the electron field operator $\hat{\varphi}(x)$ for the adjoint space is defined as

$$\hat{\varphi}^\dagger(x)=\sum_i\ \phi_i^\star(x)(\rfloor a^i)^\dagger=\sum_i\ \phi_i^\star(x)a_i\wedge,$$

and in terms of the duality between G and G^*, the regular second quantized representation of the physical operators is easily generalized,[11] e.g., using Moller–Plesset partitioning $H(\eta)=H_0(\eta)+V(\eta)$

$$H_0(\eta)=\sum_k\ \epsilon_k a_k\wedge a^k\lfloor, \tag{6}$$

and the fluctuation potential $V(\eta)$ is defined by

$$V(\eta)=\sum_i\sum_j\sum_k\sum_l\ \langle\phi_i\phi_j\|\psi_k\psi_l\rangle \times[1/4a_i\wedge a_j\wedge a^l\rfloor a^k\lfloor-\delta_{jl}\langle n_l\rangle a_i\wedge a^k\lfloor]. \tag{7}$$

The linear space of fermionlike creation and annihilation operators introduced in the superoperator formulation[26,27] of the propagator equations is now to be replaced by bi-orthonormal operator spaces[11]

$$\mathbf{h}=\{a^i\lfloor,a_i\wedge a^j\rfloor a^k\lfloor,\cdots\}\quad j<k, \tag{8}$$

$$\tilde{\mathbf{h}}=\{\rfloor a_i,\rfloor a_k\rfloor a_j\wedge a^i,\cdots\}\quad j>k, \tag{9}$$

with scalar product

$$(\tilde{h}_i|h_j)\equiv\langle\tilde{N}|[h_j,\tilde{h}_i^\dagger]_+|N\rangle. \tag{10}$$

The dilated superoperator Hamiltonian is partitioned as

$$\hat{H}(\eta)=\hat{H}_0(\eta)+\hat{V}(\eta), \tag{11}$$

with

$$\hat{H}_0X=[X,H_0(\eta)]_-,\quad \hat{V}X=[X,V(\eta)]_-,\quad \hat{I}X=X,\quad \forall X\in\mathbf{h}, \tag{12}$$

and

$$(X|Y)=\langle\tilde{N}|[Y,X^\dagger]_+|N\rangle. \tag{13}$$

The Dyson equation for the dilated bi-orthogonal matrix electron propagator $\mathbf{G}(\eta,E)$ once again is expressed as[12]

$$\mathbf{G}(\eta,E)=\langle\tilde{\mathbf{a}}|\mathbf{h}\rangle(\tilde{\mathbf{h}}|(E\hat{I}-\hat{H})|\mathbf{h})^{-1}(\tilde{\mathbf{h}}|\mathbf{a}), \tag{14}$$

and using the projection manifolds

$$\mathbf{h}=\mathbf{h}^1=\{a^i\lfloor\},\ \text{and}\ \tilde{\mathbf{h}}=\tilde{\mathbf{h}}^1\equiv\{\rfloor a_i\} \tag{15}$$

in Eq. (14) we obtain[11]

$$\mathbf{G}^0(\eta)=(\tilde{\mathbf{a}}|(E\hat{I}-\hat{H}_0(\eta))\mathbf{a})^{-1} \tag{16}$$

with

$$G^0_{ij}(\eta)=\delta_{ij}/(E-\epsilon_i), \tag{17}$$

which demonstrates the equivalence of this development to that of the undilated electron propagator. The structural equivalence at any order of perturbation theory between the dilated $G(\eta)$ and the undilated case, demonstrated by an equivalence of projection manifolds and reference state $|N\rangle$, guarantees the ease with which the dilated propagator coalesces into the undilated one for $\eta=1$ at any level of approximation.[11] For example, writing $\mathbf{h}=\mathbf{h}^1\oplus\mathbf{h}^3\oplus\mathbf{h}^5\cdots$ and $\tilde{\mathbf{h}}=\tilde{\mathbf{h}}^1\oplus\tilde{\mathbf{h}}^3\oplus\tilde{\mathbf{h}}^5\cdots$, with

$$\mathbf{h}^3=\{a_p\wedge a^a\lfloor a^b\lfloor,a_a\lfloor a^p\wedge a^q\wedge\}$$

and

$$\tilde{\mathbf{h}}^3=\{\rfloor a_b\rfloor a_a\wedge a^p,\wedge a_q\wedge a_p\rfloor a^a\},\text{etc.}, \tag{18}$$

and partitioning $\mathbf{h}=\mathbf{a}\oplus\mathbf{f}$ where $\mathbf{a}=\mathbf{h_1}$ ($a<b$ labeling occupied, $p<q$ labeling unoccupied orbitals, and i,j labeling unspecified orbitals), the dilated matrix electron propagator formulas are entirely similar to those for the undilated real electron propagator[12] except that the direct $\{\psi_i\}$ and adjoint $\{\phi_i\}$ spaces are not self dual and the bi-orthonormality permeates all expressions.

With the partitioning of the operator space $\mathbf{h}=\mathbf{a}\oplus\mathbf{f}$ the dilated electron propagator may be expressed as[12]

$$\mathbf{G}^{-1}(\eta,E)=(\tilde{\mathbf{a}}|(E\hat{I}-\hat{H}(\eta))|\mathbf{a})-(\tilde{\mathbf{a}}|\hat{H}(\eta)|\mathbf{f}) \times(\tilde{\mathbf{f}}|(E\hat{I}-\hat{H}(\eta))|\mathbf{f})^{-1}(\tilde{\mathbf{f}}|\hat{H}(\eta)|\mathbf{a}), \tag{19}$$

whereby

$$[\mathbf{G}^{-1}(\eta,\mathbf{E})]_{ij}=[\mathbf{G}_0^{-1}(\eta,\mathbf{E})]_{ij}+(\tilde{a}_i|(E\hat{I}-\hat{V}(\eta))|a_j)-(\tilde{a}_i|\hat{H}(\eta)|\mathbf{f})(\tilde{\mathbf{f}}|(E\hat{I}-\hat{H}(\eta))|\mathbf{f})^{-1}\times(\tilde{\mathbf{f}}|\hat{H}(\eta)|a_j) \quad (20)$$

$$=\mathbf{A}_0+\mathbf{A}-\mathbf{B}\mathbf{C}^{-1}\mathbf{D}, \quad (21)$$

where

$$\mathbf{A}_0=(\tilde{\mathbf{a}}|(E\hat{I}-\hat{H}_0(\eta))|\mathbf{a}), \quad (22)$$

$$\mathbf{A}=(\tilde{\mathbf{a}}|(E\hat{I}-\hat{V}(\eta))|\mathbf{a}), \quad (23)$$

$$\mathbf{B}=(\tilde{\mathbf{a}}|\hat{H}(\eta)|\mathbf{f}), \quad (24)$$

$$\mathbf{C}=(\tilde{\mathbf{f}}|(E\hat{I}-\hat{H}(\eta))|\mathbf{f}), \quad (25)$$

and

$$\mathbf{D}=(\tilde{\mathbf{f}}|\hat{H}(\eta)|\mathbf{a}). \quad (26)$$

A_0 is the Hartree–Fock electron propagator in which the reference state $|N\rangle$ is approximated by $|\mathrm{HF}\rangle$.

Our order analysis for the dilated electron propagator is similar to that for the real unscaled electron propagator[1,22,28] and proceeds by expressing the exact N electron reference state $|N\rangle$ using a Rayleigh–Schrödinger perturbation expansion with

$$|N\rangle=|\mathrm{HF}\rangle+|0^1\rangle+|0^2\rangle+\cdots, \quad (27)$$

where $|\mathrm{HF}\rangle$ is the Hartree–Fock ground state wave function, $|0^1\rangle$ is the first order Moller–Plesset correction given by

$$|0^1\rangle=\sum_{p<q}\sum_{a<b}K_{ab}^{pq}p^\dagger q^\dagger ab|\mathrm{HF}\rangle, \quad (28)$$

with

$$K_{ab}^{pq}=\frac{\langle ab\|pq\rangle}{\epsilon_a+\epsilon_b-\epsilon_p-\epsilon_q}. \quad (29)$$

a, b, c, d denote occupied orbitals, p, q, r, s denote unoccupied orbitals and i, j, k, l denote unspecified orbitals. The second order Moller–Plesset correction $|0^2\rangle$ is given by

$$|0^2\rangle=\sum_p\sum_a K_a^p p^\dagger a|\mathrm{HF}\rangle, \quad (30)$$

where

$$K_a^p=\frac{1}{2}\left[\sum_c\sum_q\sum_r\frac{\langle qr\|ca\rangle\langle pc\|qr\rangle}{(\epsilon_a-\epsilon_p)(\epsilon_c+\epsilon_a-\epsilon_r-\epsilon_q)}+\sum_c\sum_b\sum_q\frac{\langle cb\|aq\rangle\langle qp\|bc\rangle}{(\epsilon_a-\epsilon_p)(\epsilon_b+\epsilon_c-\epsilon_p-\epsilon_q)}\right]. \quad (31)$$

The contributions from the first order ($\mathbf{A}_1$) and second order ($\mathbf{A}_2$) energy independent terms are zero. The energy dependent terms in the self-energy matrix can be evaluated from $\mathbf{B}\mathbf{C}^{-1}\mathbf{D}$. To obtain the second order terms, we use the Hartree–Fock ground state to obtain $\mathbf{B}$ and $\mathbf{D}$ through first order. We separate $\mathbf{C}$ into $\mathbf{C}_0$ and $\mathbf{C}_1$ such that $\mathbf{C}=\mathbf{C}_0-\mathbf{C}_1$ where

$$\mathbf{C_0}=(\tilde{\mathbf{f}}|(E\hat{I}-\hat{H}_0(\eta))|\mathbf{f}) \text{ and } \mathbf{C}_1=(\tilde{\mathbf{f}}|\hat{V}(\eta)|\mathbf{f}). \quad (32)$$

By expansion of $\mathbf{C}^{-1}$, terms through all orders may be generated.[29] If one retains only $\mathbf{h}_3$ in $\mathbf{f}$ and approximates $|N\rangle$ by $|\mathrm{HF}\rangle$ this expansion is terminated in zeroth order and one obtains the second order (Σ^2) self-energy term $\mathbf{B}_1\mathbf{C}_0^{-1}\mathbf{D}_1$ where

$$(\mathbf{B_1})_{i,apq}=\langle ia\|pq\rangle, \quad (33)$$

$$(\mathbf{C_0})_{pqa,p'q'a'}=(E+\epsilon_a-\epsilon_p-\epsilon_q)\delta_{pp'}\delta_{qq'}\delta_{aa'}, \quad (34)$$

$$(\mathbf{D_1})_{pqa,j}=\langle pq\|ja\rangle \quad (35)$$

for the two hole one particle part resulting from the choice of $\mathbf{h}_3=\{a_p\wedge a^q\lfloor a^b\rfloor\}$ and

$$(\mathbf{B_1})_{i,pab}=-\langle ip\|ab\rangle, \quad (36)$$

$$(\mathbf{C_0})_{pab,p'a'b'}=(E+\epsilon_p-\epsilon_a-\epsilon_b)\delta_{pp'}\delta_{aa'}\delta_{bb'}, \quad (37)$$

$$(\mathbf{D_1})_{abp,j}=-\langle ab\|jp\rangle \quad (38)$$

from the two particle one hole component resulting from the choice of $\mathbf{h_3}=\{a_a\lfloor a^p\wedge a^q\wedge\}$. By multiplying the matrices $\mathbf{B}_1$, $\mathbf{C}_0^{-1}$ and $\mathbf{D}_1$, we obtain the elements of the self-energy matrix[12] correct through second order (Σ^2) which is given by

$$\Sigma_{ij}^2(\eta,E)=\frac{1}{2}\left[\sum_a\sum_b\sum_p\frac{\langle ip\|ab\rangle\langle ab\|jp\rangle}{E+\epsilon_p-\epsilon_a-\epsilon_b}+\sum_a\sum_p\sum_q\frac{\langle ia\|pq\rangle\langle pq\|ja\rangle}{E+\epsilon_a-\epsilon_p-\epsilon_q}\right], \quad (39)$$

where the antisymmetric two-electron integral

$$\langle ij\|kl\rangle=\eta^{-1}\int\psi_i(1)\psi_j(2)[(1-P_{12})/r_{12}]\times\psi_k(1)\psi_l(2)dx_1\,dx_2. \quad (40)$$

The lack of complex conjugation stems from the bi-orthonormal sets of orbitals resulting from bi-variational SCF being the complex conjugate of each other $\{\phi_i=\psi_i^*\}$.[21,23] Similarly, diagonal $2ph$-TDA decoupling of the dilated electron propagator[17] gives a formula entirely similar to that for the undilated case[2,3]

$$\Sigma_{ij}^{2ph\text{-TDA}}(\eta,E)=\frac{1}{2}\left[\sum_a\sum_b\sum_p\frac{\langle ip\|ab\rangle\langle ab\|jp\rangle}{E+\epsilon_p-\epsilon_a-\epsilon_b-\Delta_1}+\sum_a\sum_p\sum_q\frac{\langle ia\|pq\rangle\langle pq\|ja\rangle}{E+\epsilon_a-\epsilon_p-\epsilon_q-\Delta_2}\right], \quad (41)$$

where

$$\Delta_1=-\tfrac{1}{2}\langle ab\|ab\rangle+\langle bp\|bp\rangle+\langle ap\|ap\rangle$$

and

$$\Delta_2=\tfrac{1}{2}\langle pq\|pq\rangle-\langle aq\|aq\rangle-\langle ap\|ap\rangle,$$

except that the transformed two electron integrals and the orbital energies obtained from bi-variational SCF are complex.

These developments have made it obvious that the bi-orthogonal dilated electron propagator formulas are identical to those obtained for the real undilated electron propagator

except that the underlying integrals, expansion coefficients and orbital energies are complex and bi-orthonormality replaces normality. Therefore, to simplify our notations and emphasize the exact parallelism between the formulations of all bi-orthogonal dilated electron propagator and real electron propagator decouplings we shall use the prevalent notations of the real electron propagator development[3] with the complexity and bi-orthogonality being implicitly understood, e.g.,

$$p^\dagger q^\dagger ab = a_p \wedge a_q \wedge a^a \lfloor a^b \rfloor, \quad \text{and} \quad \langle \phi_i | \psi_j \rangle = \delta_{ij} \tag{42}$$

in further analysis. It is this exact parallelism of the bi-orthogonal dilated electron propagator decouplings with those of the undilated real electron propagator decouplings that separates it from other approaches to the construction of the complex scaled electron propagator[9,10] where even the second order decoupling involves more complicated formulation. Higher order and renormalized decouplings from these alternative approaches[9,10] may be still more complicated and have not been attempted.

The contribution of third order terms of **A** arises by considering the first order double excitation and second order single excitation configurations in the Rayleigh–Schrödinger expansion of the ground state wave function. The third order energy dependent part of the dilated self-energy matrix once again emerges as:

$$\mathbf{\Sigma}^3_{\mathbf{ED}}(\eta, \mathbf{E}) = \mathbf{B_2 C_0^{-1} D_1} + \mathbf{B_1 C_0^{-1} D_2} + \mathbf{B_1 C_0^{-1} C_1 C_0^{-1} D_1}, \tag{43}$$

where the subscript ED denotes energy-dependent self-energy matrix and implicit dependence of all terms in Eq. (43) on η has been suppressed. Matrices $\mathbf{B}_2$, $\mathbf{C}_0^{-1}$, $\mathbf{D}_1$ and $\mathbf{C}_1$ are evaluated with vector space $\mathbf{f}$ truncated to $\mathbf{h}_3$, i.e., $\{p^\dagger ab\}$ and $\{ap^\dagger q^\dagger\}$:

$$(\mathbf{B_2})_{i,pab} = -\frac{1}{2}\sum_q \sum_r \langle ip \| qr \rangle \langle qr \| ab \rangle' - \sum_q \sum_c \langle ic \| qa \rangle \langle qp \| bc \rangle' + \sum_q \sum_c \langle ic \| qb \rangle \langle qp \| ac \rangle', \tag{44}$$

with

$$\langle ab \| qr \rangle' = \frac{\langle ab \| qr \rangle}{\epsilon_a + \epsilon_b - \epsilon_q - \epsilon_r}, \tag{45}$$

$$(\mathbf{D_1})_{abp,j} = -\frac{1}{2}\sum_a \sum_b \sum_p \langle ab \| jp \rangle, \tag{46}$$

$$(\mathbf{C_1})_{pab,p'a'b'} = -\delta_{pp'}\langle ab' \| a'b \rangle - \delta_{aa'}\langle pb' \| p'b \rangle + \delta_{bb'}(ap \| a'p'). \tag{47}$$

By combining the appropriate matrices and using the adjoint of $\mathbf{B}_2$ and $\mathbf{D}_1$, i.e., $\mathbf{D}_2$ and $\mathbf{B}_1$, we can express the $2hp$ terms, i.e., $\mathbf{B_2 C_0^{-1} D_1}$, $\mathbf{B_1 C_0^{-1} D_2}$ and $\mathbf{B_1 C_0^{-1} C_1 C_0^{-1} D_1}$, respectively, as shown below:

$$(\mathbf{B_2 C_0^{-1} D_1})_{ij} = \frac{1}{4}\sum_a \sum_b \sum_p \sum_q \sum_r \frac{\langle ip \| qr \rangle \langle qr \| ab \rangle \langle ab \| jp \rangle}{(E + \epsilon_p - \epsilon_a - \epsilon_b)(\epsilon_a + \epsilon_b - \epsilon_q - \epsilon_r)} \tag{48}$$

$$- \sum_a \sum_b \sum_c \sum_p \sum_q \frac{\langle ic \| qb \rangle \langle qp \| ac \rangle \langle ab \| jp \rangle}{(E + \epsilon_p - \epsilon_a - \epsilon_b)(\epsilon_a + \epsilon_c - \epsilon_p - \epsilon_q)}, \tag{49}$$

$$(\mathbf{B_1 C_0^{-1} D_2})_{ij} = \frac{1}{4}\sum_a \sum_b \sum_p \sum_q \sum_r \frac{\langle ip \| ab \rangle \langle ab \| qr \rangle \langle qr \| jp \rangle}{(E + \epsilon_p - \epsilon_a - \epsilon_b)(\epsilon_a + \epsilon_b - \epsilon_q - \epsilon_r)} \tag{50}$$

$$- \sum_a \sum_b \sum_c \sum_p \sum_q \frac{\langle iq \| ac \rangle \langle ab \| pq \rangle \langle pc \| jb \rangle}{(E + \epsilon_q - \epsilon_a - \epsilon_c)(\epsilon_a + \epsilon_b - \epsilon_p - \epsilon_q)}, \tag{51}$$

$$(\mathbf{B_1 C_0^{-1} C_1 C_0^{-1} D_1})_{ij} = -\frac{1}{4}\sum_a \sum_b \sum_c \sum_d \sum_p \frac{\langle ip \| ab \rangle \langle ab \| cd \rangle \langle cd \| jp \rangle}{(E + \epsilon_p - \epsilon_c - \epsilon_d)(E + \epsilon_p - \epsilon_a - \epsilon_b)} \tag{52}$$

$$+ \sum_a \sum_b \sum_c \sum_p \sum_q \frac{\langle iq \| cb \rangle \langle cp \| aq \rangle \langle ab \| jp \rangle}{(E + \epsilon_p - \epsilon_a - \epsilon_b)(E + \epsilon_q - \epsilon_b - \epsilon_c)}. \tag{53}$$

When $\mathbf{B}_2$, $\mathbf{C}_0^{-1}$, $\mathbf{D}_1$, and $\mathbf{C}_1$ are evaluated with $\mathbf{h}_3$ as $\{ap^\dagger q^\dagger\}$, we have

$$(\mathbf{B_2})_{i,apq} = -\frac{1}{2}\sum_b \sum_c \langle ia \| bc \rangle \langle bc \| pq \rangle' - \sum_b \sum_r \langle ir \| bp \rangle \langle ba \| qr \rangle' + \sum_b \sum_r \langle ir \| bq \rangle \langle ba \| pr \rangle', \tag{54}$$

$$(\mathbf{D_1})_{pqa,j} = \frac{1}{2}\sum_p \sum_q \sum_a \langle pq \| ja \rangle, \tag{55}$$

$$(\mathbf{C_1})_{apq,a'p'q'} = +\delta_{pp'}\langle aq' \| a'q \rangle + \delta_{aa'}\langle pq' \| p'q \rangle - \delta_{qq'}\langle pa \| p'a' \rangle. \tag{56}$$

The three $2ph$ terms can be expressed as:

$$(\mathbf{B_2C_0^{-1}D_1})_{ij}=\frac{1}{4}\sum_a\sum_b\sum_c\sum_p\sum_q\sum_r \frac{\langle ic\|ab\rangle\langle ab\|pq\rangle\langle pq\|jc\rangle}{(E+\epsilon_c-\epsilon_p-\epsilon_q)(\epsilon_a+\epsilon_b-\epsilon_p-\epsilon_q)} \tag{57}$$

$$-\sum_a\sum_b\sum_p\sum_q\sum_r \frac{\langle ir\|aq\rangle\langle ab\|pr\rangle\langle pq\|jb\rangle}{(E+\epsilon_b-\epsilon_p-\epsilon_q)(\epsilon_a+\epsilon_b-\epsilon_q-\epsilon_r)}, \tag{58}$$

$$(\mathbf{B_1C_0^{-1}D_2})_{ij}=\frac{1}{4}\sum_a\sum_b\sum_c\sum_p\sum_q\sum_r \frac{\langle ia\|pq\rangle\langle pq\|bc\rangle\langle bc\|ja\rangle}{(E+\epsilon_a-\epsilon_p-\epsilon_q)(\epsilon_b+\epsilon_c-\epsilon_p-\epsilon_q)} \tag{59}$$

$$-\sum_a\sum_b\sum_p\sum_q\sum_r \frac{\langle ib\|pr\rangle\langle pq\|ab\rangle\langle ar\|jq\rangle}{(E+\epsilon_b-\epsilon_p-\epsilon_r)(\epsilon_a+\epsilon_b-\epsilon_p-\epsilon_q)}, \tag{60}$$

$$(\mathbf{B_1C_0^{-1}C_1C_0^{-1}D_1})_{ij}=\frac{1}{4}\sum_a\sum_p\sum_q\sum_r\sum_s \frac{\langle ia\|pq\rangle\langle pq\|rs\rangle\langle rs\|ja\rangle}{(E+\epsilon_a-\epsilon_r-\epsilon_s)(E+\epsilon_a-\epsilon_p-\epsilon_q)} \tag{61}$$

$$-\sum_a\sum_b\sum_p\sum_q\sum_r \frac{\langle ib\|rq\rangle\langle ra\|pb\rangle\langle pq\|ja\rangle}{(E+\epsilon_a-\epsilon_p-\epsilon_q)(E+\epsilon_b-\epsilon_q-\epsilon_r)}. \tag{62}$$

The third order energy independent dilated self-energy is also formally similar to the real undilated electron propagator[11] formulas, i.e.,

$$[\mathbf{\Sigma_{EI}^3}(\eta)]_{ij}=\sum_k\sum_l \langle \mathbf{ik}\|jl\rangle\gamma_{kl} \tag{63}$$

with

$$\gamma_{kl}=\langle N|k^\dagger l|N\rangle. \tag{64}$$

Using $|N\rangle=|\mathrm{HF}\rangle+|0^1\rangle+|0^2\rangle$ we generate the third order energy independent self-energy matrix, which is

$$[\mathbf{\Sigma_{EI}^3}(\eta)]_{ij}=\sum_k\sum_l \langle ik\|jl\rangle\langle 0^1|k^\dagger l|0^1\rangle+\sum_k\sum_l \langle ik\|jl\rangle\langle 0^2|k^\dagger l|\mathrm{HF}\rangle+\sum_k\sum_l (ik\|jl\rangle\langle \mathrm{HF}|k^\dagger l|0^2\rangle. \tag{65}$$

By expanding Eq. (65) and summing over all spins, we finally get

$$\mathbf{\Sigma_{EI}^3}(\eta)=\frac{1}{2}\sum_a\sum_b\sum_p\sum_q\sum_r \frac{\langle ir\|jp\rangle\langle ab\|rq\rangle\langle pq\|ab\rangle}{(\epsilon_a+\epsilon_b-\epsilon_p-\epsilon_q)(\epsilon_a+\epsilon_b-\epsilon_q-\epsilon_r)} \tag{66}$$

$$-\frac{1}{2}\sum_a\sum_b\sum_c\sum_p\sum_q \frac{\langle ia\|jc\rangle\langle cb\|pq\rangle\langle pq\|ab\rangle}{(\epsilon_a+\epsilon_b-\epsilon_p-\epsilon_q)(\epsilon_b+\epsilon_c-\epsilon_p-\epsilon_q)} \tag{67}$$

$$+\frac{1}{2}\sum_a\sum_b\sum_p\sum_q\sum_r \frac{\langle ip\|ja\rangle\langle ab\|qr\rangle\langle qr\|pb\rangle}{(\epsilon_a+\epsilon_b-\epsilon_q-\epsilon_r)(\epsilon_a-\epsilon_p)} \tag{68}$$

$$-\frac{1}{2}\sum_a\sum_b\sum_c\sum_p\sum_q \frac{\langle ip\|ja\rangle\langle bc\|pq\rangle\langle aq\|bc\rangle}{(\epsilon_b+\epsilon_c-\epsilon_p-\epsilon_q)(\epsilon_a-\epsilon_p)} \tag{69}$$

$$+\frac{1}{2}\sum_a\sum_b\sum_p\sum_q\sum_r \frac{\langle ia\|jr\rangle\langle rb\|pq\rangle\langle pq\|ab\rangle}{(\epsilon_a+\epsilon_b-\epsilon_p-\epsilon_q)(\epsilon_a-\epsilon_r)} \tag{70}$$

$$-\frac{1}{2}\sum_a\sum_b\sum_c\sum_p\sum_q \frac{\langle ic\|jp\rangle\langle pq\|ab\rangle\langle ab\|cq\rangle}{(\epsilon_a+\epsilon_b-\epsilon_p-\epsilon_q)(\epsilon_c-\epsilon_p)}. \tag{71}$$

The Outer Valence Green's Function (OVGF-A)[2,5] approximation is based on full third order approximation to Σ and also contains a geometric approximation for higher order contributions. No matrices need to be diagonalized. We define

$$Z=-\sum_{I=1}^{4}(\gamma_i+\kappa_i)/\Sigma^2, \tag{72}$$

where Z is a screening parameter and expressions for $\{\gamma_i\}_{i=1}^4$ and $\{\kappa_i\}_{i=1}^4$ are collected as Eqs. (48)–(51) and (57)–(60), respectively. Finally

$$\mathbf{\Sigma}_{\mathrm{OVGF}}^{\mathrm{eff}}=\mathbf{\Sigma}^2+(1+Z)^{-1}\mathbf{\Sigma}^3. \tag{73}$$

In terms of the spin-orbitals obtained from the bi-variational

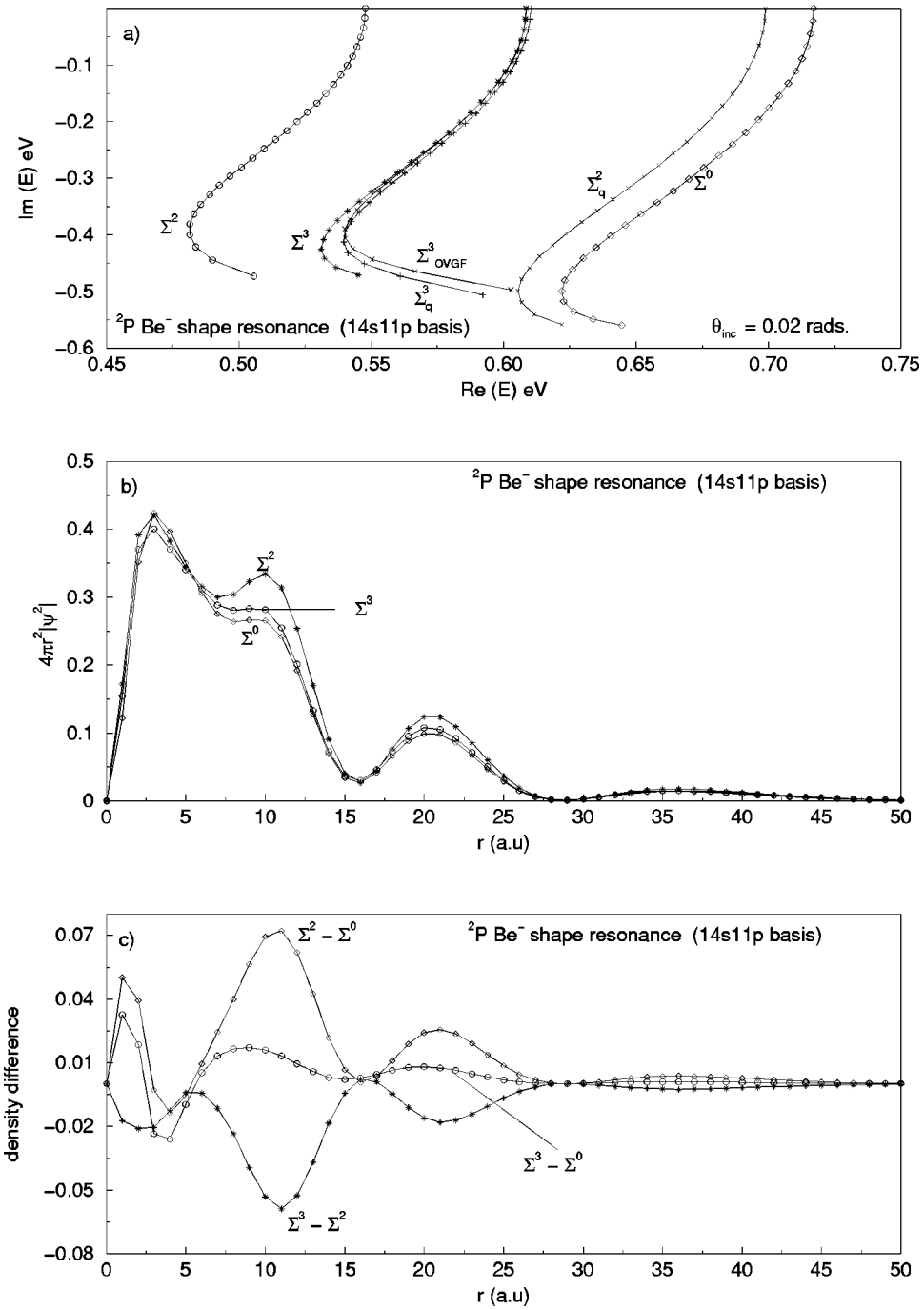

FIG. 1. (a) Theta trajectories from different decouplings of the dilated electron propagator for the ^2P Be$^-$ resonance using the $14s11p$ basis. Complex scaling parameter $\eta=\alpha e^{i\theta}$. Optimal α value (α_{opt}) is 0.915 for Σ^0, 0.8 for Σ^2, 0.9 for Σ^2_q and 0.85 for the Σ^3, Σ^3_q and Σ^3_{OVGF} decouplings. $\theta=0.0$ on the real line and θ increments are in steps of 0.02 radians. (b) Radial probability densities and (c) difference in radial probability density for the ^2P Be$^-$ resonant FDA from the Σ^0, Σ^2, and Σ^3 decouplings.

SCF procedure, combining Eqs. (17) and (20) we write the matrix electron propagator as

$$\mathbf{G}^{-1}(\eta,E)=E\mathbf{1}-\boldsymbol{\epsilon}(\eta)-\boldsymbol{\Sigma}(\eta,E)\equiv E\mathbf{1}-\mathbf{L}(\eta,E) \tag{74}$$

with Σ being the self-energy approximant resulting from chosen decoupling (Σ^2, Σ^3, $\Sigma^{2ph-\text{TDA}}$, Σ^2_q, Σ^3_q, etc.) for its construction, or in operator form

$$G(\eta,E)=(E-L(\eta,E))^{-1}, \tag{75}$$

whereby in terms of the eigenfunctions and eigenvalues of $L(\eta,E)$

$$L(\eta,E)\chi_n(\eta,E)=\mathcal{E}_n(\eta,E)\chi_n(\eta,E). \tag{76}$$

The spectral representation of G is given by

$$G(\eta,E)=(E-L(\eta,E))^{-1}\sum_n |\chi_n\rangle\langle\chi_n|$$

$$=\sum_n \frac{|\chi_n\rangle\langle\chi_n|}{E-\mathcal{E}_n(\eta,E)} \tag{77}$$

and the eigenvalues of L therefore represent the poles of G. Accordingly, the dilated electron propagator calculations proceed by iterative diagonalization

$$\mathbf{L}(\eta,E)\chi_n(\eta,E)=\mathcal{E}_n(\eta,E)\chi_n(\eta,E), \tag{78}$$

with

$$\mathbf{L}(\eta,E)=\boldsymbol{\epsilon}(\eta)+\boldsymbol{\Sigma}(\eta,E), \tag{79}$$

where $\boldsymbol{\epsilon}(\eta)$ is the diagonal matrix of orbital energies and $\boldsymbol{\Sigma}$ is the self-energy matrix from the desired decoupling. The propagator pole $\mathcal{E}$ is obtained by repeated diagonalizations such that one of the eigenvalues $\mathcal{E}_n(\eta,E)$ of $\mathbf{L}(\eta,E)$ fulfills the condition $E=\mathcal{E}_n(\eta,E)$.[12] These $\mathcal{E}_n(\eta,E)$ represent the poles of the dilated electron propagator $G(\eta,E)$. From among these poles, the resonant pole $\mathcal{E}_r(\eta,E)$ and the corresponding eigenvector (FDA) $\chi_r(\eta,E)$ are selected as per the prescription of the complex scaling theorems[7,8] whereby those roots which are invariant to changes in the complex scaling parameter η are to be associated with resonances. In a limited basis set calculation, instead of absolute stability one finds quasi-stability where the θ trajectory displays kinks, cusps, loops or inflections which indicate the proximity of a stationary point.[30] In this work the resonance attributes have been extracted from the value at the kink in θ-trajectories ($\partial\mathcal{E}_r/\partial\theta=0$). The real part of the resonant pole furnishes the energy and the imaginary part the half width of the resonance.

The quasi-particle (Σ_q^3) approximation[31] for dilated electron propagator[32] results from a diagonal approximation to the self-energy matrix $\boldsymbol{\Sigma}(\eta,E)$ with poles of the dilated electron propagator given by

$$E(\eta)=\epsilon_i+\Sigma_{ii}(\eta,E), \tag{80}$$

which are determined iteratively beginning with $E=\epsilon_i$ and Σ_{ii} may correspond to any perturbative (Σ^2,Σ^3) or renormalized decoupling like the diagonal $\Sigma^{2ph\text{-TDA}}$.

In the bi-variationally obtained bi-orthogonal orbital basis $\{\psi_i\}$, the FDA χ_n is a linear combination

$$\chi_n(\mathbf{r})=\sum_i C_{\mathrm{in}}\psi_i(\mathbf{r}), \tag{81}$$

where the mixing of the canonical orbitals allows for the incorporation of relaxation effects and nondiagonal correlation effects. In the zeroth order ($\boldsymbol{\Sigma}=\mathbf{0}$) and the quasi-particle approximations (diagonal $\boldsymbol{\Sigma}$), there is no mixing. The difference between perturbative second order (Σ^2) or renormalized diagonal $2ph$-TDA ($\Sigma^{2ph\text{-TDA}}$) decouplings manifests itself through differences between the mixing coefficients C_{in} from these approximations.

III. RESULTS AND DISCUSSION

The use of complex scaling ($\eta=\alpha e^{i\theta}$) in the characterization of resonances requires that, once uncovered, resonant poles be stable with respect to further variations in the complex scaling parameter.[7,8] However, in calculations utilizing a limited basis set only quasi-stability in a narrow range of α and θ values is observed.[30] The resonances are therefore identified by plotting the complex poles as a function of θ (theta trajectory) for optimal α and the value of the resonant pole at the inflection point (θ_{opt}) in the quasi-stable region of the theta trajectory is associated with the resonance energy (the real part) and half-width (the imaginary part). In this work, we apply the third order (Σ^3), the Outer Valence Green's Function (Σ^3_{OVGF}) and quasi-particle third order (Σ_q^3) decouplings of the dilated electron propagator to study the ^2P Be^- and the ^2P Mg^- shape and the ^2S Be^+ $(1s^{-1})$ Auger resonances. The radial density profiles of the resonant FDAs are examined to elicit information about the factors affecting the formation and decay of these resonances.

TABLE I. Energy and width of the ^2P shape resonances in e-Be scattering.

Method/reference	Energy (eV)	Width (eV)
Previous calculations:		
Static exchange phase shift (Ref. 33)	0.77	1.61
Static exchange plus polarizability phase shift (Ref. 33)	0.20	0.28
Static exchange cross section (Ref. 34)	1.20	2.6
Static exchange plus polarizability cross section (Ref. 34)	0.16	0.14
Complex ΔSCF (Ref. 35)	0.70	0.51
Singles doubles and triples complex CI (Ref. 38)	0.32	0.30
S-matrix pole (X_α) (Refs. 36, 37)	0.10	0.15
Second order dilated electron propagator based on real SCF (Ref. 10)	0.57	0.99
Bi-orthogonal dilated electron propagator (Ref. 17)	0.67	0.88
Second order/diagonal $2ph$-TDA	0.64/0.67	0.60/0.66
Present calculations: ($14s11p$ basis)		
Zeroth order	0.62	1.00
Quasi-particle second order	0.61	1.00
Second order	0.48	0.82
Quasi-particle third order	0.54	0.82
OVGF third order	0.54	0.78
Third order	0.53	0.85

The ^2P Be^- (Refs. 10, 17, 33–37) and the ^2P Mg^- (Refs. 12, 33, 34, 38–41) shape resonances have been the prototypical systems used to test the efficacy of most new approaches to the theoretical treatment of shape resonances. Similarly, the only Auger resonance to be treated using the complex scaling technique has been the ^2S Be^+ $(1s^{-1})$ Auger resonance[42,43] and these are our systems of choice as well to enable a comparison of our results with those from varied theoretical and experimental techniques.

The basis sets employed are those tested earlier[44] for effective and economic saturation both with respect to the resonance energy and width of the shape resonance in e-Be and e-Mg scattering as well as correctness of the nodal topology of the resonant FDAs.[44] The ^2P shape resonances in e-Be and e-Mg have been studied extensively and their energetics and orbital density profiles are examined first. The Auger resonances have been comparatively less well examined by complex scaling methods and results from our study of ^2S Be^+ $(1s^{-1})$ Auger attributes using three different bases and different decouplings are offered next.

A. The ^2P Be^- shape resonance

Theta trajectories from third order and other decouplings utilizing the near saturated $14s11p$ basis[44] are plotted in Fig. 1. The resonance energies and widths from the quasi-stable inflection points in these trajectories are collected in Table I along with those from other theoretical methods. It can be seen from Fig. 1 and Table I that both the energy and width obtained from the Σ^3, Σ^3_{OVGF} and Σ_q^3 decouplings are extremely close to each other and the much more economic Σ_q^3 and Σ^3_{OVGF} decouplings are equally effective. The third order

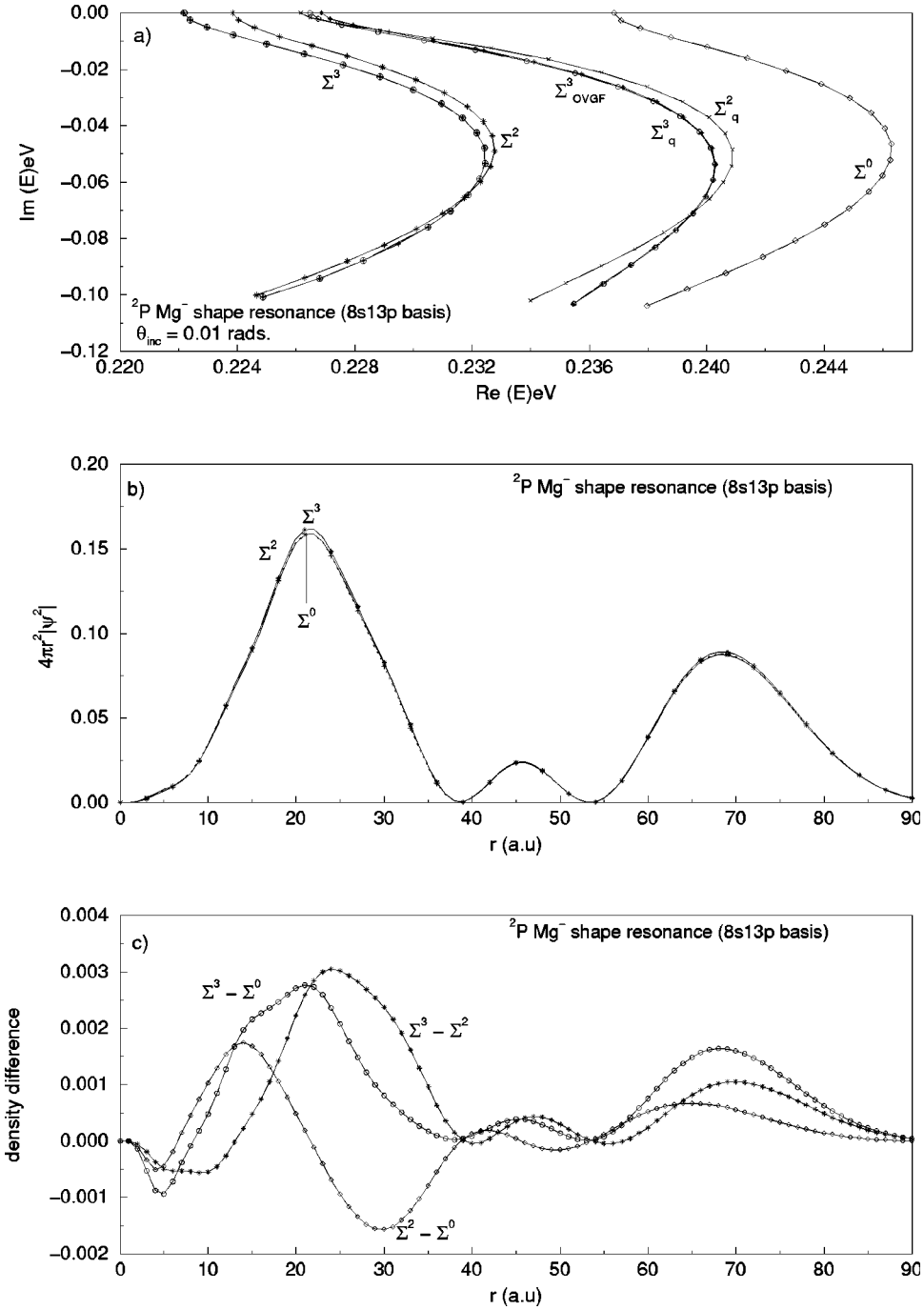

FIG. 2. (a) Theta trajectories for the ^2P Mg$^-$ resonant root from different decouplings using the $8s13p$ basis set. α_{opt} is 1.05 for Σ^0, 1.025 for Σ^2, 1.04 for Σ^2_q, 1.025 for Σ^3 and 1.04 for Σ^3_q and Σ^3_{OVGF} decouplings. (b) Radial probability density plots and (c) the difference in radial probability densities from Σ^0, Σ^2, and Σ^3 decouplings.

results fall between those from Σ^0 (bi-variational SCF) and Σ^2 decouplings and we can surmise that the Σ^3 decouplong perhaps corrects the extra stabilization (lowering of energy) provided by the Σ^2 decoupling. This feature is mirrored in the radial density profiles from decouplings presented in Fig. 1(b) where the Σ^3 density profile again is between those from the Σ^0 and Σ^2 decouplings. All of the radial density profiles have similar attributes and if we note that multiplication by r^2 exaggerates the density magnitude for large r values lifting numbers close to zero at 15 a.u. from the nucleus off the real line, the resonant orbital is primarily of $2p$ type with mixing from $3p$ and $4p$ providing for a shoulder at ~7.5 a.u. and an additional peak at 20 a.u. and nodes at ~15 a.u. and ~30 a.u. from the nucleus. These results corroborate our earlier surmise[17] that the shape resonance formation is a multi-orbital phenomenon with lower energy orbitals below the centrifugal barrier providing for binding and the higher energy orbital above the barrier assisting in its decay. The density differences plotted in Fig. 1(c) reveal an intricate redistribution of electron density over a considerably broad span of electron-nucleus distance and we infer that only primitive basis sets with sufficiently large number of both tight and diffuse GTOs can correctly describe shape resonances.

The results from a variety of theoretical approaches collected in Table I show a large scatter but if the somewhat unrealistic results from Static Exchange Phase Shift[33] and Static Exchange Cross-Section[34] are neglected (it is difficult

TABLE II. Energy and width of the ^2P shape resonances in *e*-Mg scattering.

Method/reference	Energy (eV)	Width (eV)
Experiment (Ref. 39)	0.15	0.13
Previous calculations:		
Static exchange phase shift (Refs. 33, 34)	0.46/0.46	1.37/1.53
Static exchange plus polarizability phase shift (Refs. 33, 34)	0.16/0.14	0.24/0.24
Static exchange cross section (Ref. 34)	0.91	2.30
Static exchange plus polarizability cross section (Ref. 34)	0.19	0.30
CI (Ref. 40)	0.20	0.23
S-matrix pole (X_α) (Refs. 36, 37)	0.08	0.17
Complex ΔSCF (Ref. 41)	0.51	0.54
Dilated electron propagator based on real SCF (Ref. 45)	0.14	0.13
Second order (Ref. 17)	0.15	0.13
Diagonal *2ph*-TDA (Ref. 17)	0.15	0.13
Present calculations: ($8s13p$ basis)		
Zeroth order	0.25	0.10
Quasi-particle second order	0.24	0.10
Second order	0.23	0.10
Quasi-particle third order	0.24	0.10
OVGF third order	0.24	0.10
Third order	0.23	0.10

to see a resonance centered at 0.77 eV with a width of 0.80 eV on both sides); all other results can be taken to describe various parts of the same resonant wave packet centered at ~0.54 eV and a width of ~0.42 eV on both sides. The saturated nature of our basis and high order (Σ^3) of the decoupling employed here gives us confidence that this system which has not been investigated experimentally so far due to its toxic nature, if experimented with should give the attributes elicited from this investigation.

B. The ^2P Mg^- shape resonance

The ^2P Mg^- shape resonance is a well characterized[39] system which has been extensively studied using many different theoretical techniques.[17,33,34,36,37,40,41,45] The theta trajectories from different decouplings in Fig. 2(a) and the radial density profiles from Fig. 2(b) show that this is indeed a prototype shape resonance with electron density peaking at 22 a.u. to provide loose binding which does not disturb the other electrons and with considerable amplitude also at large distances facilitating decay. The lack of change between Σ^0, Σ^2 and Σ^3 decoupling results confirms the classic picture of shape resonance as temporary electron attachment in an empty orbital without initiating major relaxation and correlation in the target. As seen in Fig. 2(c), the different decouplings do lead to variations in density distribution but the small magnitude of these changes has minimal impact on resonance energies and widths which are almost identical (Table II). Although, some second order dilated electron propagator calculations including our own[46] provide energy and width in much better agreement with the experimental results this has been shown[44,45] to be serendipitous and the Σ^3 results presented here may be taken to be a benchmark for dilated electron propagator calculations.

C. The ^2S Be^+ ($1s^{-1}$) Auger resonance

One of the major advantages of the electron propagator formalism is its unique ability to provide information about both electron attachment and detachment from a single calculation.[1–6] Apart from the ^2P Be^- shape resonance, the ^2S Be^+ ($1s^{-1}$) Auger resonance has also served as a prototypical system to investigate the effectiveness of different theoretical schemes in the investigation of Auger resonances.[42,43,47] Application of the third order decoupling of the dilated electron propagator to the ^2S Be^+ Auger resonance is therefore an obvious adjunct for ascertaining its utility and, to begin with, we used the $14s11p$ basis employed earlier for the investigation of the ^2P Be^- shape resonance to investigate the $1s^{-1}$ Auger hole as well. The θ-trajectories for the $1s^{-1}$ Auger hole from Σ^2, Σ^2_q, Σ^3 and Σ^3_q decouplings using the $14s11p$ basis are plotted in Fig. 3(a) and the values for the energy and width obtained from the quasistable portion of the theta trajectories along with experimental and some other theoretical results are collected in Table III. Since the second order energy and width obtained using this basis set was at large variance with those obtained using other theoretical approaches[42,47] and an earlier second order dilated electron propagator calculation employing a different ($10s6p$) basis,[43] we repeated the Σ^3_q and Σ^3 calculations using the $10s6p$ basis and the $16s6p$ basis obtained from the $10s6p$ basis by uncontracting all CGTOs in the *s*-block. The theta trajectories from the $10s6p$ and $16s6p$ bases are presented in Figs. 3(b) and 3(c) and the energy and width from all the three ($14s11p$, $10s6p$ and $16s6p$) bases have been collected in Table III. As can be seen from Figs. 3(a)–(c) the much more economic quasi-particle decouplings closely parallel the Σ^2 and Σ^3 decouplings and therefore results from the Σ^2_q and Σ^3_q decouplings have not been tabulated separately.

The large impact of both the basis set variations and the order of the decoupling is easily seen from the results listed in Table III. The basis set effects within the same order and difference between results obtained from different decouplings for the same basis ($\Sigma^2-\Sigma^3$) are considerably large for all the three bases with the difference between results from the $14s11p$ and the $10s6p$ bases being remarkable both for the energy and the width. The lowering of 0.29 eV in energy and increase of 0.54 eV in width induced by the Σ^3 decoupling for the $14s11p$ basis in comparison to the Σ^2 results from the same basis underscores the importance of correlation and relaxation effects incorporated by the Σ^3 decoupling. The Σ^3 result for the $16s6p$ basis provides the theoretical resonance energy (124.09 eV) closest to the experimental value obtained so far. However, even with the Σ^3 decoupling and a fairly large $16s6p$ basis the theoretical results are 0.46 eV higher than the experimental results. The width obtained with the $16s6p$ basis and the Σ^3 decoupling, however, is larger than those obtained using other theoretical methods.[42,43,47]

An attempt to understand these differences has been made by plotting the radial probability densities for the resonant FDA from different bases and decouplings corresponding to the $1s^{-1}$ Auger pole. To begin with, we have plotted

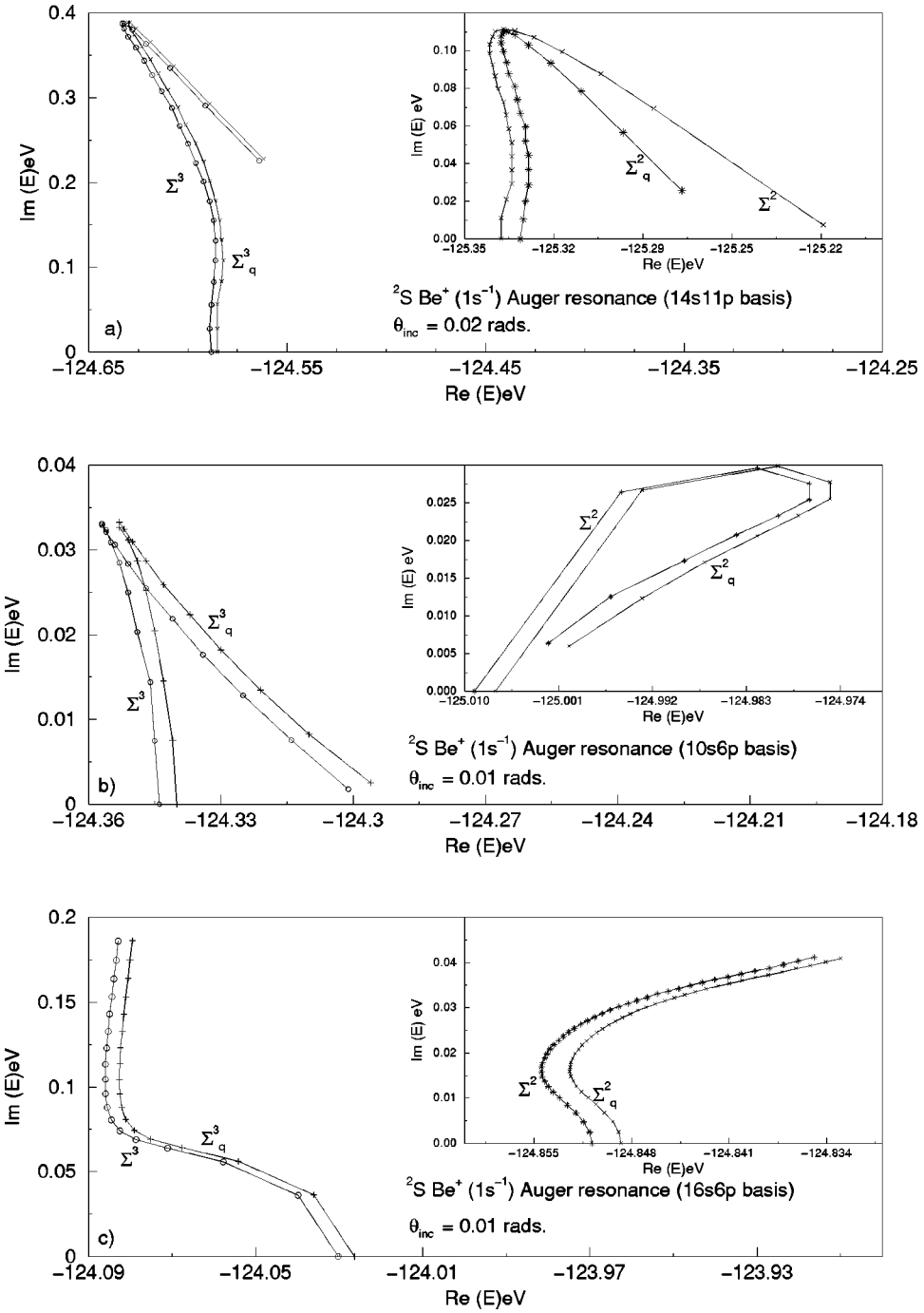

FIG. 3. Theta trajectories from different decouplings of the dilated electron propagator for the ^2S Be$^+$ $(1s^{-1})$ resonant FDA using: (a) $14s11p$ basis. α_{opt} is 0.85 for all the decouplings. (b) $10s6p$ basis. α_{opt} is 0.85 for Σ^2, Σ^2_q, and 0.93 for Σ^3 and Σ^3_q decouplings. (c) $16s6p$ basis. α_{opt} is 0.89 for Σ^3 and Σ^2_q and 0.86 for Σ^3 and Σ^3_q decouplings.

the radial density for the $Be^{+++}(1s)$ [Energy $=(4)^2*13.6\,\text{eV}=217\,\text{eV}$] labeled *Ref* and those from the resonant $1s^{-1}$ FDAs from the Σ^3 decoupling for all the three bases in Fig. 4(a). That the resonant FDA isolated by the Σ^3 decoupling is of the $1s$ type is evident from the radial density profiles from all the three bases plotted in Fig. 4(a). The difference between the hydrogenic Be^{+++} reference density and those from the $1s^{-1}\Sigma^3$ FDAs from different bases has been plotted in Fig. 4(b) and the crucial role of relaxation in lowering of binding energy from 217.6 eV in Be^{+++} to ~124.3 eV in Be $(1s)$ is clearly brought out by depletion of electron density from the vicinity of the nucleus and its buildup farther away. The radial density profiles from different bases in Fig. 4(a) look identical on the scale of the plot but as can be seen from Fig. 4(c) and Table III, the difference of $\sim 10^{-3}$ in radial density magnitude can translate into a difference of ~0.3 eV in the binding energy. The magnitude of difference between radial distribution profile from different bases in Fig. 4(c) correlates well with the differences in energy and widths obtained from them. The higher order decouplings provide for greater relaxation and thereby lowering of resonance (binding) energy and this is shown by the radial and difference density plots from the Σ^0, Σ^2 and Σ^3 decouplings for the $14s11p$ basis in Figs. 5(a) and 5(b), respectively. The different decouplings play an identical role for the $10s6p$ and $16s6p$ bases as well and these profiles have therefore not been displayed separately.

The effect of complex scaling and the changes in radial

TABLE III. Energy and width of the Be^+ $(1s^{-1})$ ^2S Auger resonance.

Method/reference	Energy (eV)	Width (eV)
Experiment (Refs. 50, 51)	123.63	⋯
Previous calculations:		
Many-body perturbation theory (Ref. 47)	⋯	0.09
Second order electron propagator with Siegert boundary condition (Ref. 42)	125.47	0.02
Second order dilated electron propagation (Ref. 43)	124.98	0.05
Present calculations: ($14s11p/10s6p/16s6p$)		
Second order	125.34/124.98/124.85	0.22/0.05/0.03
Third order	124.63/124.35/124.09	0.76/0.07/0.22

density profiles accompanying uncovering of resonances for optimal η are traced by plotting density profiles for the Σ^3 decoupling from the different bases for $\theta=0.0$ (on the real line) for $\eta=\alpha=1.0$ in Fig. 5(c) and for $\eta=\alpha_{\text{opt}}$ in Fig. 5(d). The difference densities plotted in Fig. 5(e) underline the role of optimal α in stabilizing the resonance by providing superior relaxation and comparatively more balanced nature of the $10s6p$ basis in the characterization of the $1s^{-1}$ resonance may be attributed to the lower relaxation required by change in α from $\alpha=1.0$ to $\alpha=\alpha_{\text{opt}}$ for this basis. The trends correlate well with the corresponding binding energies collected in Table IV.

It can also be seen from Table IV that the difference between binding energy obtained using $\alpha=1.0$ and $\alpha=\alpha_{\text{opt}}$ is minimal and very close to the energy values listed in Table III for η_{opt}. The shift from real line ($\theta=0.0$) into complex plane to uncover the resonance at $\alpha=\alpha_{\text{opt}}$ and $\theta=\theta_{\text{opt}}$ may therefore be taken to impact mostly on the width. The resonance is fully uncovered in the complex plane for $\alpha=\alpha_{\text{opt}}$ and $\theta=\theta_{\text{opt}}$ (i.e., $\eta_{\text{opt}}=\alpha_{\text{opt}}e^{i\theta_{\text{opt}}}$) and an attempt to study the effect of basis sets and decouplings on the width is made by plotting the radial density profiles for different decouplings and the difference between densities for the Σ^2 and Σ^3 decouplings for the $14s11p$ basis in Figs. 5(f) and 5(g) and the difference between the resonant FDAs from Σ^3 decoupling using the $14s11p$ basis ($\alpha_{\text{opt}}=0.85$, $\theta_{\text{opt}}=0.38$ radians) and $10s6p$ basis ($\alpha_{\text{opt}}=0.93$, $\theta_{\text{opt}}=0.08$ radians) in Fig. 5(h). The inference that can be drawn from this limited investigation is that the bases and decouplings forcing a larger confinement of electron density near the nucleus, i.e., providing lesser relaxation destabilise the resonance by forcing both the $1s$ electrons to share a smaller spatial span thereby lowering its lifetime and increasing its width. However a more systematic and extensive investigation of the basis set effects for Auger resonances is required and we conclude by repeating that the desirable basis set attributes for treating shape and Auger resonances seem to be different and the basis set and the higher order decouplings which incorporate greater relaxation and correlation effects are much more critical to the description of Auger resonances. Also, just as in the case of shape resonances, the quasi-particle decouplings provide almost identical values for the energy and width of the Auger resonance as well and these more economic decouplings can be utilized with advantage. However, the mechanistic investigation based on radial density plots from the resonant amplitudes requires the full decouplings since the diagonal quasi-particle decouplings do not provide for the mixing of orbitals. We believe that determination of η_{opt} from a much more economic Σ_q^3 theta trajectory followed by construction of full Σ^3 propagator only for the single η_{opt} value may be a reasonable and economic alternative.

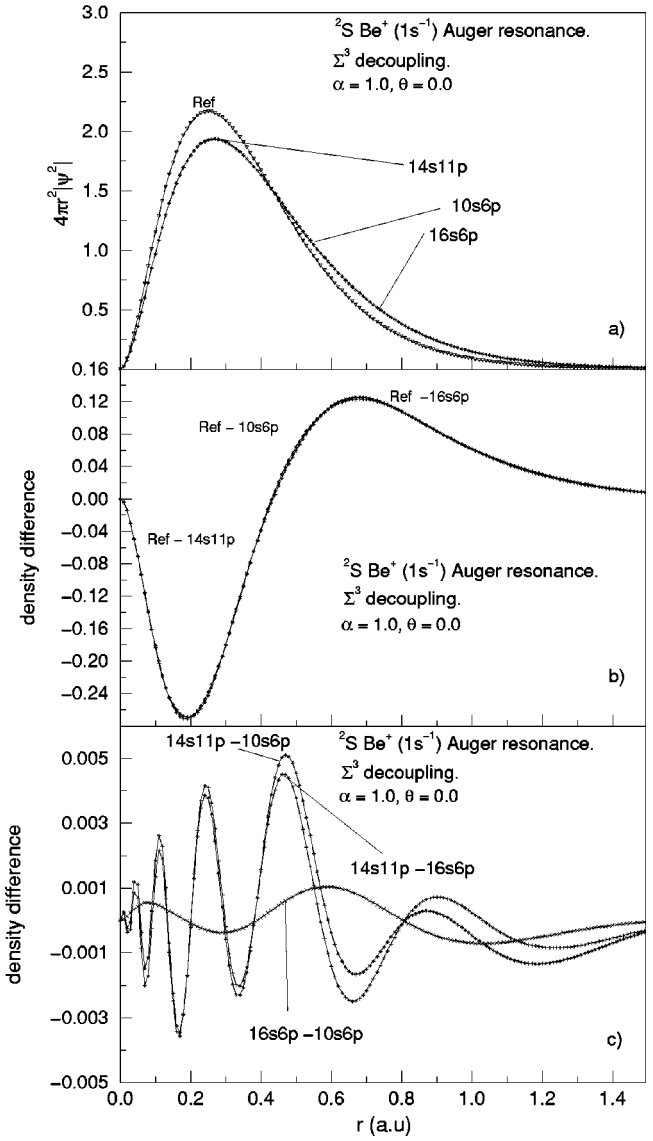

FIG. 4. (a) Radial probability densities and (b) difference in radial probability density for the ^2S Be^+ $(1s^{-1})$ resonant FDA from the $14s11p$, $10s6p$ and $16s6p$ basis sets obtained using Σ^3 decoupling and the hydrogenic $Be^{+++}1s$ orbital. (c) Difference in radial probability density for the resonant $1s^{-1}\Sigma^3$FDA using the $14s11p$, $10s6p$ and $16s6p$ basis sets.

IV. CONCLUDING REMARKS

The third order, the related quasi-particle and Outer Valence Green's Function (OVGF) decouplings of the biorthogonal dilated electron propagator have been formulated and implemented for the first time. Investigation of the prototypical ^2P Be^- and ^2P Mg^- shape and the ^2S Be^+ $(1s^{-1})$

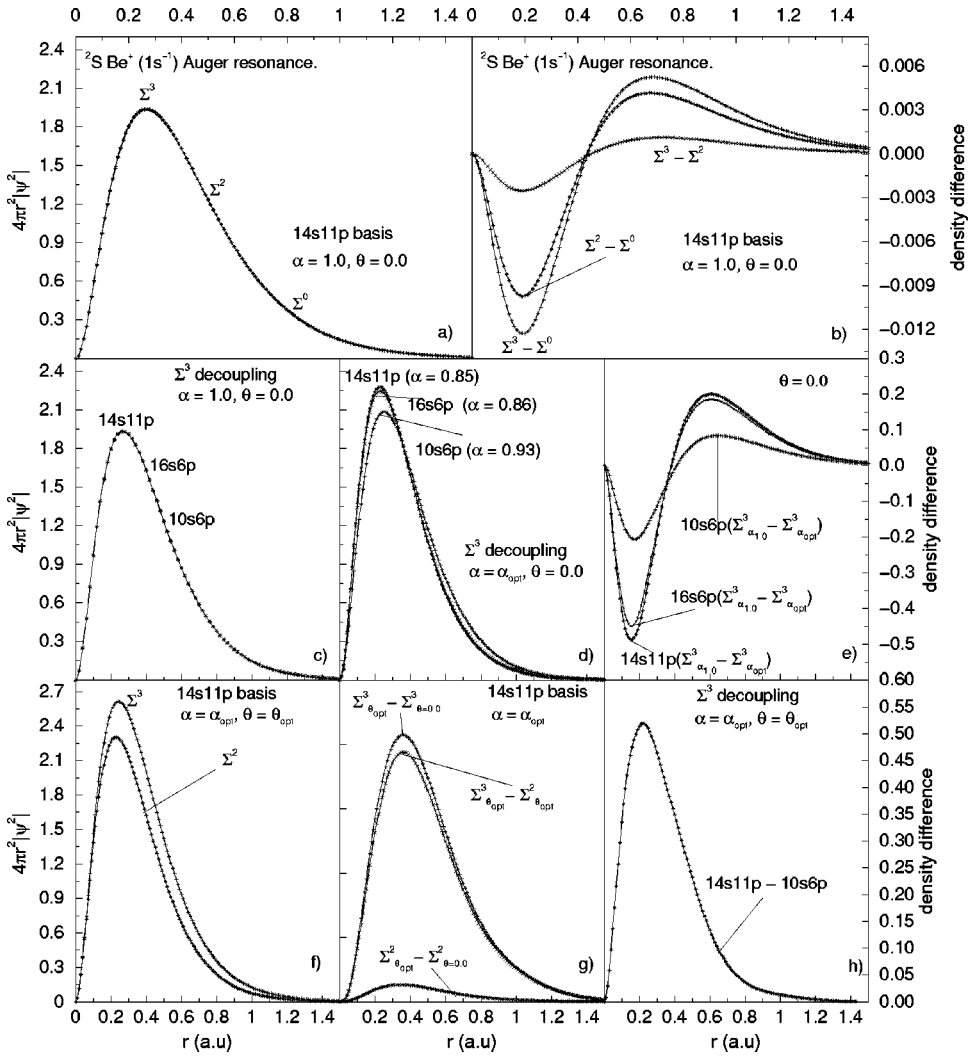

FIG. 5. (a) Radial probability density and (b) difference density for the $^2S\ \mathrm{Be}^+\ (1s^{-1})$ resonant FDA from different decouplings employing the $14s11p$ basis. Radial probability densities at $\alpha=1.0$ (c) and $\alpha=\alpha_{\mathrm{opt}}$ (d). Difference in radial densities from the Σ^3 decoupling using the $14s11p$, $10s6p$ and $16s6p$ bases (e). Radial probability densities at $\alpha=\alpha_{\mathrm{opt}}$, $\theta=\theta_{\mathrm{opt}}$ (f), difference in radial probability densities at $\alpha=\alpha_{\mathrm{opt}}$ using Σ^2 and Σ^3 decouplings from $14s11p$ basis (g), and difference in radial probability densities between the $14s11p$ and $10s6p\Sigma^31s^{-1}$ resonant FDAs($\eta=\eta_{\mathrm{opt}}$) (h).

Auger resonances using the Σ^3 and Σ^3_q decouplings show different extent of improvement to the energy and the width calculated using the second order decoupling alone. The much more economical Σ^3_q decoupling provides value for the energies and the widths almost identical to those from the much more demanding full Σ^3 decoupling. However, the Σ^3_q approximant being diagonal, does not provide for mixing of orbitals required for redistribution of electron density and thereby a complementary test of the effectiveness of different decouplings. The second order decoupling provides almost identical results for energy and width of the $^2P\ \mathrm{Be}^-$ and $^2P\ \mathrm{Mg}^-$ shape resonances which are close to those for the third order (Σ^3) decoupling but the third order FDAs incorporate additional correlation and relaxation effects which provide for subtle redistribution of electron density to accommodate the contradictory pulls of binding and decay required for accurate description of resonances. The proximity of energy and width obtained from different decouplings for the $^2P\ \mathrm{Be}^-$ and the $^2P\ \mathrm{Mg}^-$ shape resonances lends credence to the simple picture of shape resonance resulting from electron attachment unaccompanied by large disturbances in the target. However, we should add that although the energies from different decouplings are similar there are subtle differences in the corresponding electron density distributions and the energy alone may be not be a sufficiently sensitive test of the efficacy of these decouplings.

TABLE IV. Be ($1s$) binding energy on the real line ($\theta=0.0$) for $\alpha=1.0$ and $\alpha=\alpha_{\mathrm{opt}}$.

Method/reference	$\alpha=1.0$	$\alpha=\alpha_{\mathrm{opt}}$
Present calculations: ($14s11p/10s6p/16s6p$)		
Zeroth order	128.78/128.80/128.76	128.78/128.70/128.75
Second order	125.37/124.96/124.87	125.34/125.01/124.85
Third order	124.72/124.38/124.22	124.59/124.34/124.03

The Auger resonances resulting from a core hole necessitate considerable redistribution of electron density and the Σ^3 decoupling as expected provides superior agreement with the experimental result. These results, however, are sensitive to the choice of primitive basis and a limited study of basis set effects undertaken reveals that the primitive bases providing a reasonable description of Auger resonances may differ considerably from those optimized for describing shape resonances and a methodical study of the type undertaken for shape resonances[44] will be useful. For Auger resonances, the Σ^3 decoupling provides large correction to results obtained using the Σ^2 decoupling alone and recommends itself for

investigation of other atomic/molecular Auger resonances.

The best value for the $(1s^{-1})$ Be^{+} Auger resonance energy obtained using the Σ^3 decoupling is, however, still 0.46 eV higher than the experimental value and application of an infinite order renormalized decoupling like the full $2ph$-TDA[15] is appealing. However, due to the large dimension of the $\mathbf{h}_3$ manifold, the full $2ph$-TDA requires either inversion of a very large complex **C** matrix [Eqs. (21) and (25)] using a full diagonalization to obtain all eigenvectors or repeated diagonalizations of the superoperator Hamiltonian matrix[1] **H**. Even for modest basis sets, both **C** and **H** will have a very large dimension with the largest block even after exploiting spatial and spin symmetry most likely to be of the order of 10^3 and higher and repeated diagonalizations of these large complex matrices for many values of E and $\sim$150 different values of η is much too demanding. Furthermore, although the full $2ph$-TDA is complete in second order, it is incomplete in third and higher orders and since the choice of the superoperator metric[1] required to obtain the $2ph$-TDA and Σ^3 decouplings are quite different, a simple algebraic reconciliation to obtain a biorthogonal ADC(3)[2] type extension may not be easy to formulate. A new[48] variant seems promising but nonavailability of Davidson's type diagonalization algorithms applicable to large non-hermitian complex symmetric matrices coupled with the need for iterative construction for many ($\sim$150) η values keeps it out of our reach for the time being. The matrices constructed for the Σ^3 decoupling can provide a partial fourth order (Σ_p^4) correction[28,49] and an attempt to incorporate the (Σ_p^4) decoupling for a more accurate treatment of Auger resonances is an obvious extension of this work. An effort along these lines is underway in our group.

ACKNOWLEDGMENT

We are pleased to acknowledge financial support from the Department of Science and Technology, India (Grant No. SP/S1/H26/96).

[1] J. V. Ortiz, Adv. Quantum Chem. **35**, 33 (1999).
[2] W. von Niessen, J. Schirmer, and L. S. Cederbaum, Comput. Phys. Rep. **1**, 57 (1984).
[3] Y. Öhrn and G. Born, Adv. Quantum Chem. **13**, 1 (1981).
[4] M. F. Herman, K. F. Freed, and D. L. Yeager, Adv. Chem. Phys. **48**, 1 (1981).
[5] L. S. Cederbaum and W. Domcke, Adv. Chem. Phys. **36**, 205 (1977).
[6] J. Simons, Annu. Rev. Phys. Chem. **28**, 15 (1977).
[7] W. P. Reinhardt, Annu. Rev. Phys. Chem. **33**, 223 (1982).
[8] B. R. Junker, Adv. At. Mol. Phys. **18**, 207 (1982).
[9] P. Winkler, Z. Phys. A **291**, 199 (1977).
[10] R. A. Donnelly and J. Simons, J. Chem. Phys. **73**, 2858 (1980).
[11] M. Mishra, P. Froelich, and Y. Öhrn, Chem. Phys. Lett. **81**, 339 (1981).
[12] M. K. Mishra and M. N. Medikeri, Adv. Quantum Chem. **27**, 223 (1996).
[13] S. Mahalakshmi and M. K. Mishra, Chem. Phys. Lett. **296**, 43 (1998).
[14] A. Venkatnathan and M. K. Mishra, Chem. Phys. Lett. **296**, 223 (1998).
[15] J. Schirmer and L. S. Cederbaum, J. Phys. B **11**, 1889 (1978); *ibid.* **11**, 1901 (1978).
[16] G. Born and Y. Öhrn, Chem. Phys. Lett. **61**, 397 (1979).
[17] M. N. Medikeri, J. Nair, and M. K. Mishra, J. Chem. Phys. **99**, 1869 (1993).
[18] M. N. Medikeri and M. K. Mishra, Proc. Ind. Acad. Sci., Chemical Sciences **106**, 111 (1994).
[19] J. V. Ortiz, J. Chem. Phys. **87**, 1701 (1987); *ibid.* **102**, 295 (1995); *ibid.* **108**, 1008 (1998); Chem. Phys. Lett. **136**, 387 (1987).
[20] J. V. Ortiz, J. Chem. Phys. **92**, 6728 (1990).
[21] M. Mishra, Y. Öhrn, and P. Froelich, Phys. Lett. A **84**, 4 (1981).
[22] R. Longo, B. Champagne, and Y. Öhrn, Theor. Chim. Acta **90**, 397 (1995).
[23] P. O. Löwdin, P. Froelich, and M. K. Mishra, Adv. Quantum Chem. **20**, 185 (1989).
[24] P. O. Löwdin, P. Froelich, and M. K. Mishra, Int. J. Quantum Chem. **2**, 867 (1989).
[25] P. Froelich, Quantum Theory Project, Univ. of Florida, preprint, TF 582, 1980, unpublished.
[26] O. Goscinski and B. Lukman, Chem. Phys. Lett. **7**, 573 (1970).
[27] B. T. Pickup and O. Goscinski, Mol. Phys. **26**, 1013 (1973).
[28] P. Jorgensen and J. Simons, *Second Quantization Based Methods in Quantum Chemistry* (Academic, New York).
[29] J. V. Ortiz, J. Chem. Phys. **89**, 6348 (1988).
[30] N. Moiseyev, S. Friedland, and P. R. Certain, J. Chem. Phys. **74**, 4739 (1981).
[31] L. S. Cederbaum, J. Phys. B **8**, 290 (1975); Theor. Chim. Acta **31**, 239 (1973).
[32] M. N. Medikeri and M. K. Mishra, Chem. Phys. Lett. **211**, 607 (1993).
[33] H. A. Kurtz and Y. Öhrn, Phys. Rev. A **19**, 43 (1979).
[34] H. A. Kurtz and K. Jordan, J. Phys. B **14**, 4361 (1981).
[35] C. W. McCurdy, T. N. Rescigno, E. R. Davidson, and J. G. Lauderdale, J. Chem. Phys. **73**, 3268 (1980).
[36] P. Krylstedt, M. Rittby, N. Elander, and E. J. Brändas, J. Phys. B **20**, 1295 (1987).
[37] P. Krylstedt, N. Elander, and E. J. Brändas, J. Phys. B **21**, 3969 (1988).
[38] C. W. McCurdy and J. F. McNutt, Chem. Phys. Lett. **94**, 306 (1983).
[39] P. D. Burrow, J. A. Michedja, and J. Comer, J. Phys. B **9**, 3255 (1976).
[40] A. U. Hazi, J. Phys. B **11**, L259 (1978).
[41] C. W. McCurdy, J. G. Lauderdale, and R. C. Mowrey, J. Chem. Phys. **75**, 1835 (1981).
[42] M. Palmquist, P. L. Altick, J. Ritcher, P. Winkler, and R. Yaris, Phys. Rev. A **23**, 1795 (1981).
[43] M. Mishra, O. Goscinski, and Y. Öhrn, J. Chem. Phys. **79**, 5505 (1983).
[44] A. Venkatnathan, M. K. Mishra, and Hans Jørgen Aa. Jensen, Theor. Chem. Acc. (in press).
[45] R. A. Donnelly, J. Chem. Phys. **76**, 5414 (1982).
[46] M. Mishra, H. A. Kurtz, O. Goscinski, and Y. Öhrn, J. Chem. Phys. **79**, 1896 (1983).
[47] H. P. Kelly, Phys. Rev. A **9**, 1582 (1974).
[48] J. V. Ortiz, J. Chem. Phys. **109**, 5741 (1998).
[49] J. V. Ortiz, Int. J. Quantum Chem. **S22**, 431 (1988).
[50] P. Bisgaard, R. Bruch, B. Fatrup, and M. Rødbro, Phys. Scr. **17**, 49 (1978).
[51] M. Rødbro, R. Bruch, and P. Bisgaard, J. Phys. B **12**, 2413 (1979).